Preparation and Characterization of Magnetite/Hydroxyapatite/Chitosan Nanocomposite by *In Situ* Compositing Method

Wei Cui, Qiaoling Hu, Jia Wu, Baoqiang Li, Jiacong Shen

Institute of Polymer Composites, Zhejiang University, Hangzhou 310027, People's Republic of China

Received 9 February 2007; accepted 30 July 2007
DOI 10.1002/app.28013
Published online 2 May 2008 in Wiley InterScience (www.interscience.wiley.com).

ABSTRACT: Chitosan is an important kind of biomaterial that is widely used in medical applications. One of the key concerns about its use is the preparation of composites used for bone engineering. Aim of this study concerns the preparation of three-dimensional nanocomposites having potential use in bone repair and regeneration. The magnetite/hydroxyapatite/chitosan nanocomposites were prepared via *in situ* compositing method by preparing precursor solutions and molds with chitosan membrane. These nanocomposites were characterized by chemical, spectroscopic, magnetic, and morphological methods. X-ray diffraction analysis results demonstrate the formation of magnetite and hydroxyapatite in the chitosan matrix. FTIR analysis indicates that inorganic nanoparticles were chemically bound to the amino and hydroxyl groups in CS molecules. From TG/DTA data, it can be concluded that during preparation raw materials were almost perfectly incorporated into the nanocomposites, and the decrease in decomposition temperatures indicates the formation of chemical bonds between inorganic nanoparticles and chitosan molecules. TEM results show that the maximum size of inorganic particles in the magnetite/hydroxyapatite/chitosan nanocomposites was under 50 nm, and these particles were dispersed homogeneously in the chitosan matrix. From the magnetic measurement, it could be concluded that the nanocomposites were superparamagnetic, which is also the peculiarity of nanomagnetites. © 2008 Wiley Periodicals, Inc. J Appl Polym Sci 109: 2081–2088, 2008

Key words: chitosan; magnetism; hydroxyapatite; nanocomposite; *in situ* compositing; magnetic polymers; nanotechnology

INTRODUCTION

In the field of biomaterials science, the development of new materials for effective repair of the bone is an important objective. Bone is a kind of composite materials made up of 60–70% inorganic mineral crystals and 30–40% organic matrix consisting mostly of collagen protein fibers and the major mineral component of bone is hydroxyapatite in the form of tiny elongated crystal.[1,2] Current bone implant research primarily focuses on two directions: (1) coating on metallic implants, (2) organic-inorganic composites. The current coated metallic implants have provided a superior mechanical implant anchorage, but they are also associated with the problems including stress shielding of the surrounding bone and poor durability of the coatings over time. Biocomposites based on a biodegradable polymer matrix reinforced with hydroxyapatite have showed enhancement of the osteogenic and good ability to prevent the migration of hydroxyapatite. Because of these factors, great attention has been focused on the biomaterial in conjugation with natural polymers and synthetic polymers.[3,4] Markak and William Clyne[5] proved that magneto mechanical could stimulate bone growth in a bonded array of ferromagnetic fibers. Takegami et al.[6] prepared ferromagnetic bone cement by blending magnetite power and silica glass power with resin which could be used for local hyperthermia in skeletal system. Also the magnetic therapy on the healing of bone fractures was studied by Baibekov and Khanapiyaev.[7] The preparation and application of magnetic polymer composites are of great interest for biomedical application.[8] For such applications, it is necessary that the composite should be biocompatible, nontoxic, and biodegradable.

Magnetite (Fe_3O_4) is widespread in the environment, despite the fact that it is thermodynamically unstable with respect to hematite (α-Fe_2O_3) in the presence of oxygen. It was widely used in targeted delivery of drugs,[9] MRI reagent,[10] hyperthermia treatment,[11] and many other areas. But recent studies mainly focus on the zero-dimensional microspheres, and there is less study on three-dimensional magnetic biomaterials compared with micro-spheres.

Correspondence to: Q. Hu (huql@zju.edu.cn).
Contract grant sponsor: National Natural Science Foundation of China; contract grant numbers: 50173023, 50333020, 50773070.
Contract grant sponsor: Foundation Research Project of China; contract grant number: 2005CB623902.

TABLE I
Composition of the As-Prepared Fe_3O_4/HA/CS Nanocomposites

Composite	Component (mass ratio) (CS/Fe_3O_4/HA)	Fe_3O_4		HA	CS	
		Fe^{2+} (mmol)	Fe^{3+} (mmol)	Ca^{2+} (mmol)	$H_2PO_4^-$ (mmol)	CS (g)
a	95 : 2.5 : 2.5	2.15	4.30	4.98	2.99	19.0
b	90 : 5 : 5	4.30	8.60	9.96	5.98	18.0
c	95 : 5 : 0	4.30	8.60	0	0	19.0
d	95 : 0 : 5	0	0	9.96	5.98	19.0

Hydroxyapatite (HA) with the chemical formula $Ca_{10}(PO_4)_4OH)_6$ has been extensively used for hard tissue replacement and augmentation due to its biocompatibility and osteoconductive potential.[12] However, this material is difficult to shape into the specific forms required for bone substitution due to its hardness and brittleness. Combining biopolymer with minerals to give a biomaterial with the toughness and flexibility of the biopolymer and the strength and hardness of the mineral filler has its origin in nature, such as shell and crab. In virtue of this inspiration, composites of HA and bioorganic polymers that can overcome these problems have ignited great interest.[13]

Chitosan (CS), poly-β(1,4)-2-amino-2-deoxy-D-glucose, is the partly deacetylated product of chitin, which can be extracted from crustacean and insects. It was suggested to be used in orthopedic application to provide temporary mechanical support for the regeneration of bone cell ingrowth owing to its good biocompatible, nontoxic, biodegradable, and inherent wound healing characteristics.[14] In recent years, incorporation of CS with biominerals has aroused mounting interest for the preparation of biomaterials.[15]

A critical obstacle in assembling and maintaining nanoscaled materials from nanoparticle clusters is the tendency of the latter to aggregate to reduce the energy associated with a high ratio of surface area to volume. The aim of the present study is to prepare Fe_3O_4/HA/CS nanocomposite with inorganic materials dispersed homogenously in the CS matrix via an *in situ* compositing method. The properties of the as-prepared nanocomposites have been investigated by transmission electron microscopy (TEM), powder X-ray diffraction, Fourier-transformed infrared (FTIR) spectroscopy. Magnetic measurement was carried out in a DC extraction magnetometer at room temperature in physical properties measurement system (PPMS). Thermo gravimetric analysis (TGA) was performed using a TG Q500 of Thermo Analyses (TA) apparatus.

EXPERIMENTS

Materials

Chitosan powder (biomedical grade, viscosity average molecular weight 34×10^4, degree of deacetylation is about 91%). $FeCl_2{\cdot}4H_2O$, $FeCl_3{\cdot}6H_2O$, $Ca(NO_3)_2{\cdot}4H_2O$, KH_2PO_4, and NaOH were of analytic grade and used without further purification, acetic acid solution (2% v/v) was self prepared.

Preparation of Fe_3O_4/HA/CS nanocomposites

Appropriate amount of CS powder was added to 2% acetic acid solution under vigorous agitation for half an hour. Then the mixed solution of Ca $(NO_3)_2{\cdot}H_2O$ and KH_2PO_4 with the molar ratio of Ca^{2+} to $H_2PO_4^-$ of 1.67 was added to the CS solution. Then the obtained mixed solution was stirred for another half an hour at room temperature. After that, $FeCl_2$ solution was fleetly added to the as-prepared solution. After 15 min of vigorous agitation, the $FeCl_3$ solution was also added, and the molar ratio of Fe^{2+} to Fe^{3+} was 0.5. At last, the resulting solution was vigorously stirred for 2 h, and then the obtained rufous solution was held for 12 h to remove the air bubbles trapped in it during stirring. Table I shows the composition of the Fe_3O_4/HA/CS precursory solution.

Cylindrical Fe_3O_4 /HA/CS nanocomposites were prepared as follows: Pure CS solution (5% m/v, about 5 mL) was cast uniformly into a mold and the superfluous solution was poured out, then the mold was soaked in 5% (wt/v) NaOH solution for about an hour to deposit a layer of pure CS membrane on the internal surface of the mold. The precursory solution of Fe_3O_4/HA/CS nanocomposites was poured into the mold, and then soaked in 5% (wt/v) NaOH solution for about 1 min. The mold was taken away, and the obtained gel nanocomposites were soaked in 5% (wt/v) NaOH solution for 24 h. Then the gel nanocomposites were washed with distilled water until the pH value of the composites' surface was 7. Finally, the nanocomposites were put in an oven and dried at 60°C for about 24 h, and the black nanocomposites with length 80–90 mm and diameter 4.5–5.0 mm were obtained. Figure 1 is the flow chart of the preparation of Fe_3O_4/HA/CS nanocomposites.

X-ray diffraction analysis

Phase purity and crystallographic studies of the samples were carried out with a powder X-ray diffractometer (Rigaku D/max 2550PC) using a monochro-

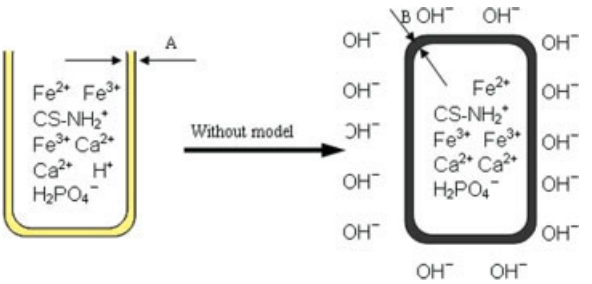

Figure 1 The flow chart for preparing Fe_3O_4/HA/CS nanocomposites. [Color figure can be viewed in the online issue, which is available at www.interscience.wiley.com.]

matic Cu Kα radiation generated at 40 kV, 300 mA, scanning rate 10°/min.

TEM evaluation

Microstructure and sizes of inorganic particles dispersed in the CS matrix of the samples were observed by TEM (JEOL, Japan, JEM-1200EX).

Infrared analysis

Infrared analysis of the samples was carried out by an FTIR spectrophotometer over the range between 4000 and 400 cm^{-1}.

Magnetic measurement

Magnetic measurement was performed by using a PPMS-9 magnetometer at 298 K.

Thermal analysis

The TGA of the nanocomposites was studied on each powder sample using a TG Q500 of TA apparatus and measurements were recorded from 50 to 700°C at 10°C/min heating rate in air.

RESULTS AND DISCUSSION

In the production of Fe_3O_4/HA/CS nanocomposite, *in situ* compositing method at room temperature was preferred, because through this method inorganic fillings could disperse homogeneously in the chitosan matrix, which could give significant help to the improvement of the bending strength of the materials compared with blending method. In addition, chitosan, as most cellulosic materials, begins to decompose at 200°C in air, precluding the use of melt extrusion or injection molding method.

Mechanism of formation of Fe_3O_4/HA/CS nanocomposites by *in situ* compositing

During the preparation of precursory solution it was related to several ions, and it was difficult to obtain the coexistence of all ions without further disposal, especially because Fe^{3+} can react with $H_2PO_4^-$, HPO_4^{2-} to form $FePO_4$ deposition, and the mechanism can be explained by following equations,

$$Fe^{3+} + HPO_4^- + CH_3COO^- \rightleftharpoons FePO_4 \downarrow + CH_3COOH$$

$$Fe^{3+} + H_2PO_4^- + 2CH_3COO^- \rightleftharpoons FePO_4 \downarrow + 2CH_3COOH$$

$FePO_4$ dissolves in dilute inorganic acid, but cannot dissolve in acetic acid. So to avoid the formation of $FePO_4$, the pH value of the precursory solution was adjusted below 1, which ensured the coexistence of all ions. In the Fe_3O_4/HA/CS precursory solution, the amino groups of chitosan were protonated to $—NH_3^+$; the process could be expressed as follows:

$$CS—NH_2 + HAc \longrightarrow CS—NH_3^+ + Ac^-$$

Chitosan has good chelate ability thanks to the presence of nitrogen in amino groups, which can coordinate with ions having hollow orbits such as Fe^{2+},[16] Fe^{3+},[17] Ca^{2+}[18] to form chelates, that is to say it can mobilize ions in the chitosan matrix and form reaction positions. The chitosan membrane used in this experiment was osmotic,[19] so small ions (OH^-, Ac^-) can penetrate through the CS membrane owing to the concentration gradient, whereas chitosan chains cannot pass due to the entwisting of chains. When the OH^- ions migrate into the Fe_3O_4/HA/CS precursory solution though chitosan membrane, they will encounter protonated chitosan, Fe^{2+}, Fe^{3+}, Ca^{2+}, and $H_2PO_4^-$, and the following reactions occur, resulting in the aggradations of chitosan, Fe_3O_4, and HA.

$$CS—NH_3^+ + OH^- \longrightarrow CS—NH_2 \downarrow + H_2O$$

$$Fe^{2+} + 2\,Fe^{3+} + 8OH^- \longrightarrow Fe_3O_4 \downarrow + 4H_2O$$

$$10Ca^{2+} + 6H_2PO_4^- + 14OH^- \longrightarrow Ca_{10}(PO_4)_6(OH)_2 \downarrow + 12H_2O$$

In this method of preparing nanocomposites, the pure chitosan membrane has two functions: firstly, it can load the precursory solution to form the required shapes; secondly, the rate of immigration of OH^- can be controlled by the pure chitosan membrane, and the acid-based neutralization reactions were put under control due to the dependence on the concentration gradient of OH^-. The mechanism of the compositing process was shown in Figure 2.

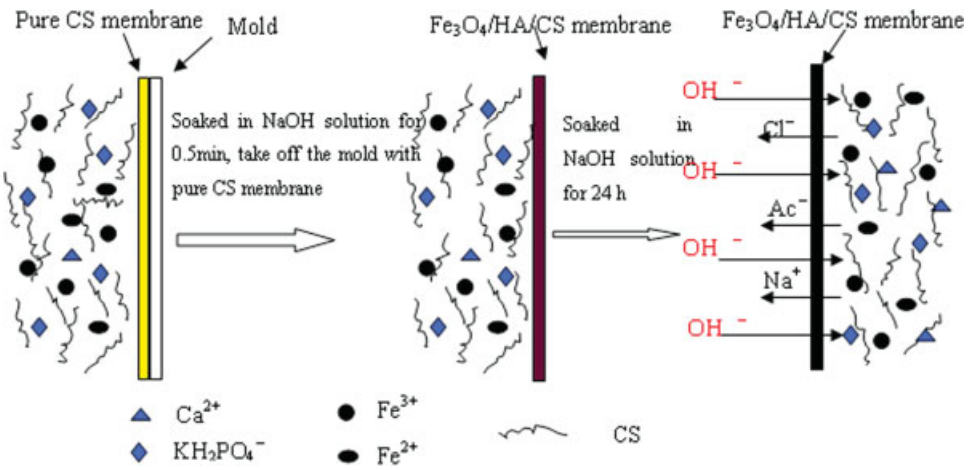

Figure 2 The mechanism of Fe_3O_4/HA/CS nanocomposites preparation via *in situ* compositing method. [Color figure can be viewed in the online issue, which is available at www.interscience.wiley.com.]

Because of the structure of gel nanocomposites, any irons trapped in could be easily washed away by circularly distilled water. When in the oven, solid state appeared during the evaporation of the water trapped in the gel nanocomposites, solid/liquid interface was replaced by solid/gas interface with higher energy. To prevent the energy increasing, the water should evaporate forth to cover the solid/gas interface. The liquid volume decreased along with the evaporation, so for the sake of covering the gas/liquid interface, the gas/liquid interface must be bended. For cylindrical cores, the engendered tensile force can be calculated as follows,

$$P = \frac{2\gamma_{LV}\cos\theta}{r_p}$$

where γ_{LV}: gas/liquid interface energy; θ: the contact angle; r_p: radius of the cores.

As tensile force acts on the liquid, the phase of saturated liquid turns into compressed state, and there will be two results,[20] (a) According to Darcy, water is inclined to evaporate forth along the gradient stress. (b) The tensile force will be balanced by the stress induced by contraction of the gel nanocomposites, when the osmosis of the gel nanocomposites decreases, the evaporation becomes difficult, and the shrink rate in the surface is inclined to be faster than that in the interior. As a result, the nanocomposites can be self-reinforced by the drying stress formed by these different strains.

X-ray diffraction analysis

Figure 3 showed a series of typical X-ray patterns of pure chitosan, Fe_3O_4/CS, HA/CS and Fe_3O_4/HA/CS nanocomposites. Pure chitosan [Fig. 3(a)] shows a strong reflection at about 19.7°and a relatively weak reflection centering at around 10°, which are associated with the crystalline regions and have been used to estimate crystallinity.[21] For the Fe_3O_4/CS [Fig. 3(b)], HA/CS [Fig. 3(d)] and Fe_3O_4/HA/CS [Fig. 3(c,e)] samples, the broad peaks with poor crystallinity around the characteristic region near to 26° and 32° (2θ) were due to the formation of HA, and 32° overlapped diffractions of 300, 211, and, 112.[22] By comparing to standard card, the three major crystalline peaks at 2θ = 35.64°, 46.7°, and 63.07° were assigned to Fe_3O_4 based on the preparation methods. The highest peak that appeared approximately at 20° was assigned to CS, and the peak strength was weaker when the inorganic content increased compared with pure chitosan, which suggested there might be a significant reduction in the crystalline in the as-prepared nanocomposites. This was probably due to the effect of cations introduced into CS matrix by the amino and hydroxyl group of chitosan that destroyed the orientation of chitosan chains formed by the intermolecular and intramolecular H-bonding

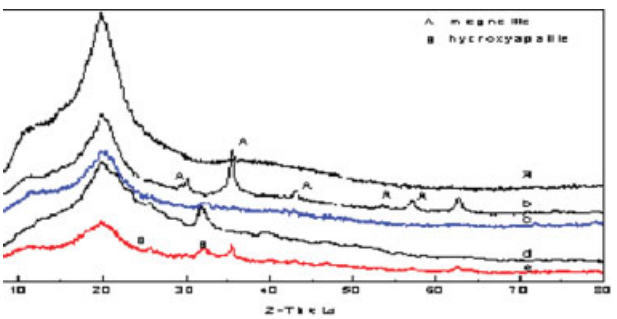

Figure 3 X-ray diffraction patterns for as-prepared nanocomposites, (a) pure chitosan, (b) Fe_3O_4/CS (5/95), (c) Fe_3O_4/HA/CS (2.5/2.5/90), (d) HA/CS(5/95), (e) Fe_3O_4/HA/CS (5/5/90). [Color figure can be viewed in the online issue, which is available at www.interscience.wiley.com.]

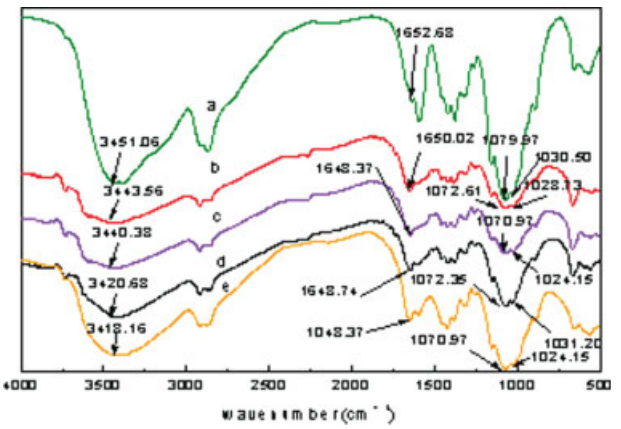

Figure 4 FTIR spectra for as-prepared nanocomposites, (a) pure chitosan, (b) Fe_3O_4/HA/CS (2.5/2.5/90), (c) Fe_3O_4/CS (5/90), (d) Fe_3O_4/HA/CS (5/5/95), (e) HA/CS (5/90). [Color figure can be viewed in the online issue, which is available at www.interscience.wiley.com.]

effect. These findings will be assigned in the FTIR findings in the following sections.

FTIR analysis

Figure 4 showed the FTIR spectra of pure chitosan, Fe_3O_4/CS, HA/CS, and Fe_3O_4/HA/CS nanocomposites with various ratios. Pure chitosan had characteristic absorption bands around 3451 cm^{-1} and 1653 cm^{-1}, revealing the stretching vibration of amino group bonded to the hydroxyl group in chitosan, and the amino bending mode in the primary amine respectively, and the absorption bands of amide II were located around 1554 cm^{-1}. The stretching vibration bands of secondary hydroxyl groups and hydroxyl ions were around 1080^{-1} and 1030 cm^{-1}. In comparison with the pure chitosan, the nanocomposites showed the following major differences, (a) the absorption bands at 3451 cm^{-1} and 1653^{-1} cm^{-1} were weakened with the increase of inorganic content. This suggested the existence of function between the added metallic ions and amino groups, and the formation of coordination bond. Because of the formation of coordination bond, the electron cloud of N in the amino groups moved toward the metallic ions resulting in the weakening of N—H strength, and the stretching vibration and bending energy decreased, so the absorption peaks of N—H shifted toward lower frequency values depending on the incorporated inorganic content. (b) The absorption bands at 1030 cm^{-1} and 1080 cm^{-1} were weakened with the increase of inorganic content. This suggested the hydroxyl groups in chitosan also participated in the formation of coordination bond. In general, chitosan-metal chelates can be formed by amino and hydroxyl groups in chitosan with metallic ions having hollow orbits.[23] Therefore, it is suggested that the chemical interaction resulting in the formation of chelates in the precursory solution is attributed to the coordination bond of chitosan-metallic ions.

Thermal analysis

Figures 5 and 6 show the TG-DTA curves of pure chitosan and Fe_3O_4/HA/CS nanocomposites with various ratios, respectively. For pure chitosan materials, the sample weight rapidly decreased with increasing temperature, and the degradation took place in three stages. The first stage began at ~85°C with weight loss of 10.17%; the second stage started at about 225°C and reached a maximum at about 303°C, with weight loss of 47%; the third stage finished at about 550°C, with weight loss of about 41.88%. The first stage could be attributed to the loss of water present in the chitosan material, and this

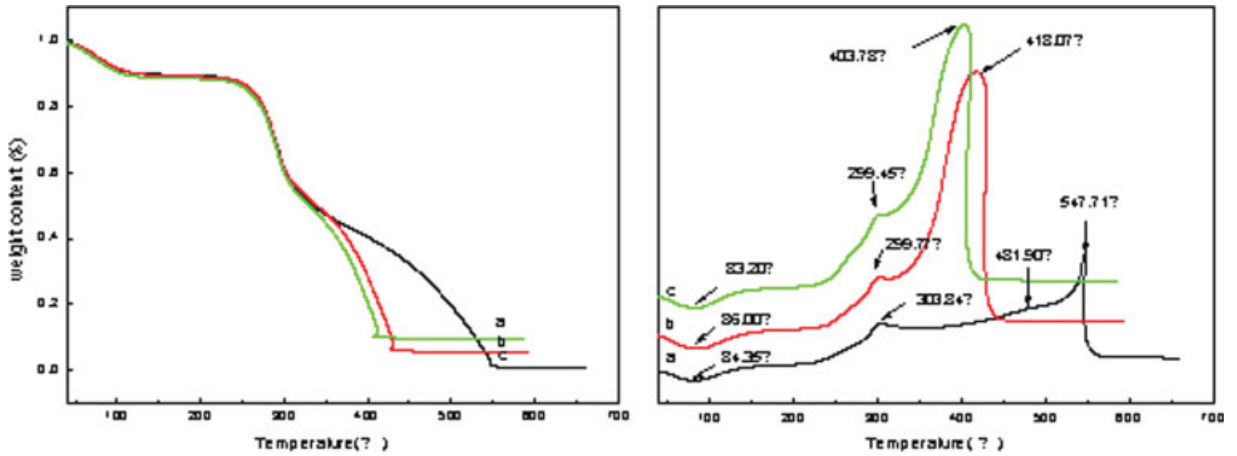

Figure 5 TGA/DTA curves for pure chitosan and Fe_3O_4/HA/CS nanocomposites of (a) pure CS, (b) 2.25/2.5/95, (c) 5/5/10 in the 40–700°C temperature range under an air atmosphere. [Color figure can be viewed in the online issue, which is available at www.interscience.wiley.com.]

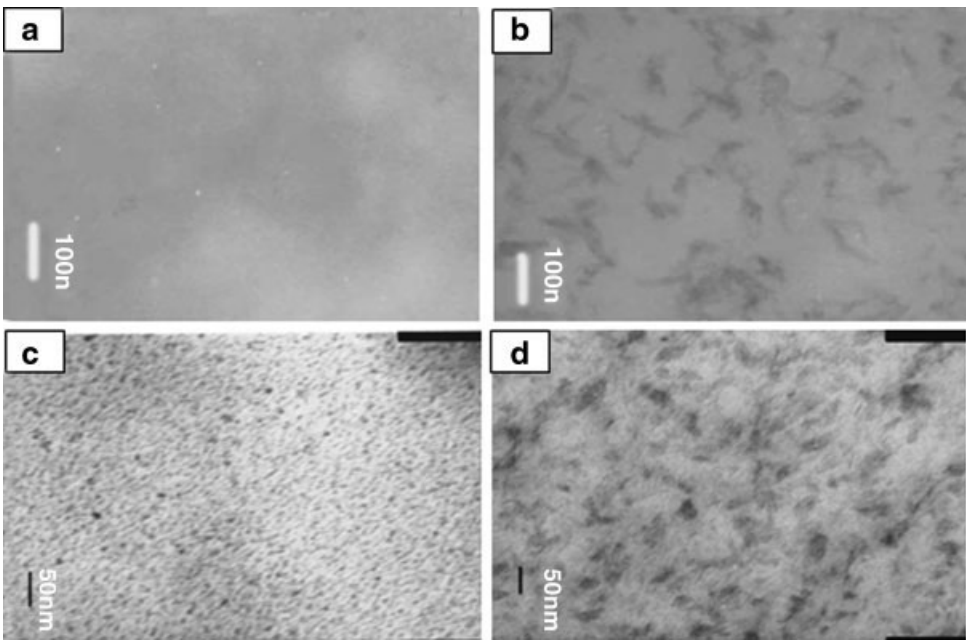

Figure 6 TEM micrographs of Fe_3O_4/HA/CS nanocomposites, (a) pure chitosan (b) Fe_3O_4/CS (w/w) = 5/95, (c) HA/CS (w/w) = 5/95, (d) Fe_3O_4/HA/CS (w/w/w) = 2.5/2.5/90.

view could be supported by the fact that a broad endothermic peak was observed around 80°C in DTA curves. From the TGA curves of pure chitosan material, three exothermic peaks were obtained during the second and third degradation stages. The first exothermic peak was due to the degradation of chitosan, whereas the second broad peak may result from the thermal degradation of a new crosslinked material formed by thermal crosslinking reactions that occurred in the first stage of degradation process. Pawlak and Mucha[24] have confirmed that the crosslinking of chitosan macromolecules follows the destruction of amino groups. The third decomposition stage, which appears at about 550°C, may be due to the burning up of chitosan. TG/TGA curves of Figure 5(b,c) are somewhat different from those of pure chitosan, but three thermal degradation stages were also obtained. The first water-loss stage started at about 60°C and reached a maximum at 86°C, with weight loss of about 10.5% and 11.1%. The second and third degradation stages started at about 299°C and 425°C, with weight loss of 83.7% and 78.9%, and the maximum temperature (418°C) was lower than that of chitosan (547.7°C).The decomposition temperature was found to decrease with increasing inorganic content, and the results supported the existence of chemical actions between inorganic and CS in Fe_3O_4/HA/CS. In the nanocomposites very tiny nanoparticles are dispersed homogeneously in CS matrix as shown by TEM analysis in Figure 6. It can be concluded from FTIR results that the inorganic nanoparticles were chemically bound to amino groups and hydroxyl groups in CS molecules. That is to say in these samples a lot of organic–inorganic chemical bonds between inorganic phases and CS molecules were formed, and the effect of chitosan crossing-linking was weakened in the first degradation stage. As the TG curves did not show a weight change above 700°C, the chitosan and inorganic content in the nanocomposites were determined from the weight loss between 50°C and 700°C, as given in Table II. However, the mass increase caused by oxidation of Fe_3O_4 could not be observed in the TG curves, which may be due to the fact that the content

TABLE II
Composition of Fe_3O_4/HA/CS Nanocomposite Measured by TG-DTA

No.	Fe_3O_4/HA/CS preparation (weight ratio)	Samples via TG-DTA measurement		
		H_2O (wt %)	Chitosan (wt %)	Inorganic content (wt %)
a	0/0/100	10.17	88.8	0
b	2.5/2.5/95	10.51	83.87	5.31
c	5/5/90	11.18	78.87	9.33

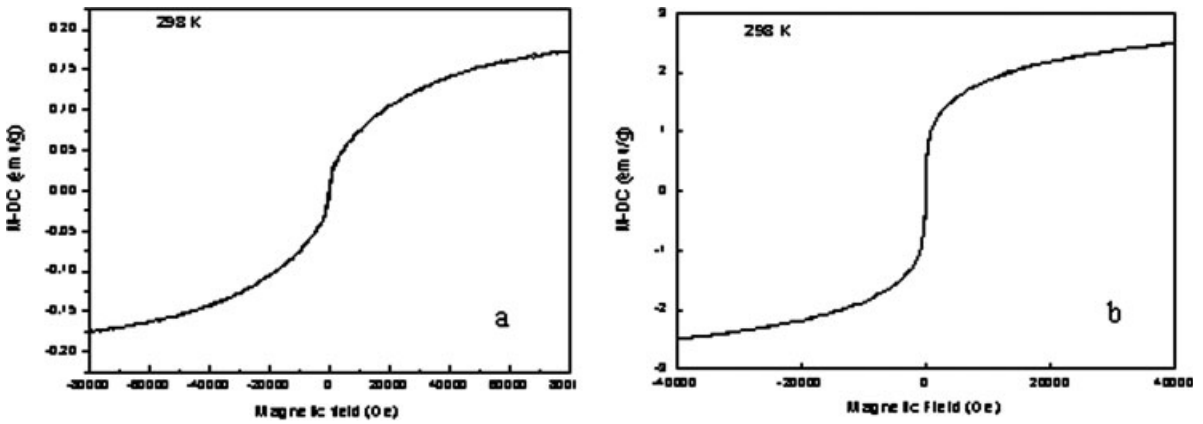

Figure 7 Magnetic hysteresis of Fe_3O_4/HA/CS nanocomposites at 298 K, (a) Fe_3O_4/HA/CS (w/w/w) = 2.5/2.5/95, (b) Fe_3O_4/HA/CS (w/w/w) = 5/5/90.

of Fe_3O_4 was small, and the increase value could be conversed according to the equation,

$$Fe_3O_4 + 1/4O_2 \longrightarrow 3/2\ Fe_2O_3$$

The chitosan content was found to be almost consistent with the initial addition during the preparation, and the inorganic content formed were almost in keeping with the stoichiometric ratio; therefore, it is believed that during the preparation raw materials were almost perfectly incorporated into the nanocomposites.

Morphology of the nanocomposites

Figure 6 shows the TEM micrographs of pure chitosan (a), Fe_3O_4/CS (b), HA/CS (c), and Fe_3O_4/HA/CS (d). As can be seen in Figure 6(a,b), many global particles are found in Fe_3O_4/CS composite and they disperse homogeneously in the chitosan matrix. The typical size of the particles is about 10 nm, and the particle size distribution is narrow, so no obvious aggregations are observed and this is the strongpoint of *in situ* method when compared with blending method in composites preparation. Figure 6(c) shows the nanosized particles dispersed well in the CS matrix with a typical size of about 100 nm in length, 20–30 nm in width. As can be seen in Figure 6(d), the shape of particles is different from those shown in Figure 6(b,c); the particles with the maximal size of 40 nm were also dispersed well in the chitosan matrix, and no aggregations formed, but it could not distinguish Fe_3O_4 from HA nanoparticles, which may be due to the intergrowth of inorganic particles in chitosan matrix.

Magnetic properties of the nanocomposites

The magnetic properties of Fe_3O_4/HA/CS nanocomposites were studied at 298 K. Bulk Fe_3O_4 is ferromagnetic at room temperature, but below a critical particle size Fe_3O_4 becomes superparamagnetic and shows no remanence or coercivity.[25] According to superparamagnetic theory, when the dimension of magnetic particles reduces, to maintain the lowest energy state, the number of magnetic domain border will also decrease, through to single domain particles without inner magnetic domain border. If the dimension of the single domain particles decreases to being under a critical dimension D_p (superparamagnetic critical dimension), and the added magnetic field is zero, magnetization intensity becomes zero. With aggrandizement of the added magnetic field, magnetization intensity augments fleetly, and the superparamagnetic phenomena appears. The D_p value of magnetite is 25 nm.[26] Figure 7 shows the hysteresis loop of the samples, the coercivity and remanence values are not discernible at 298 K, indicating a superparamagnetic behavior. The saturation magnetizations (M_s) of the prepared nanocomposites were smaller when compared with that of bulk Fe_3O_4 (92 emu/g), which may be likely due to the mutual action between Fe_3O_4, HA and CS, and also the existence of a surface layer with reduced magnetizations.[27]

CONCLUSION

Novel superparamagnetic nanocomposites with various Fe_3O_4/HA/CS ratios were prepared using *in situ* compositing method. The Fe_3O_4 and HA nanoparticles with maximum sizes under 50 nm dispersed homogeneously in the nanocomposites obtained, chemical bonds between inorganic materials and CS molecules were also formed. Future work is aimed at characterizing the mechanical properties and osteoconductive potential of the Fe_3O_4/HA/CS nanocomposites *in vivo* by added magnetic field.

References

1. Rhee, S. H.; Suetsugu, Y.; Tanaka, J. Biomaterials 2001, 22, 2843.
2. Ramesh S. Malays J Chem 2001, 3, 0035.
3. Bigi, A.; Boanini, E.; Panzavolta, S.; Roveri, N.; Rubini K. J Biomed Mater Res 2002, 59, 709.
4. Wang, M.; Joseph, R.; Bonfield, W. Biomaterials 1998, 19, 2357.
5. Markaki, A. E.; William Clyne, T. W. T. Biomaterials 2004, 25, 4805.
6. Takegami, K.; Sano, T.; Wakabayashi, H.; Sonoda, J.; Yamazaki, T.; Morita, S.; Shibuya, T.; Uchida, A. J Biomed Mater Res 1998, 43, 210.
7. Baibekov, I. M.; Khanapiyaev, U. Kh. Bull Exp Biol Med 2001, 131, 399.
8. Ajay, K. G.; Mona, G. Biomaterials 2005, 26, 3995.
9. Ramazan, A.; Michael A. Z.; Richard, O. C.; Judy, S. R. J Magn Magn Mater 2005, 292, 108.
10. Oswald, P.; Clement, O.; Chambon, C.; Schouman-Claeys, E. Magn Reson Imaging 1997, 15, 1025.
11. Takegami, K.; Sano T.; Wakabayashi, H.; Sonoda, J.; Yamazaki T.; Morita S.; Shibuya T.; Uchida A. J Biomed Mater Res 1998, 43, 210.
12. Sarawathy, G.; Pal, S.; Rose, C.; Sastry T. P. Bull Mater Sci 2001, 24, 415.
13. Andrew, C. A.; Wan, E. K.; Hastings, G. W. J Biomed Mater Res 1997, 38, 235.
14. Ito, M.; Hidaka, Y.; NakaJima, M.; Yagasaki, H.; Kafrawy, A. H. J Biomed Mater Res 1999, 45, 204.
15. Muzzarelli, C.; Muzzarelli, R. A. A. J Inorg Biochem 2002, 92, 89.
16. Subhash, C.; Bhatia, N. R. Biomacromolecules 2003, 4, 723.
17. Bhatia, S. C.; Ravi, N. Biomacromolecules 2000, 1, 413.
18. Yamaguchi, I.; Tokuchi, K.; Fukuzaki, H.; Koama, Y.; Takakuda, K.; Monma, H.; Tanaka, J. J Biomed Mater Res 2001, 55, 20.
19. Qiaoling, H.; Baoqiang, L.; Mang, W.; Jiacong, S. Biomaterials 2004, 25, 779.
20. White, L. R. J Colloid Interface Sci 1982, 90, 536.
21. Harish Prashanth, K. V.; Kittur, F. S.; Tharanathan R. N. Carbohydr Polym 2002, 50, 27.
22. Murugan, R.; Ramakrishna S. Biomaterials 2004, 25, 3829.
23. Inoue, K.; Baba Y. J Ion Exchange 1997, 8, 115.
24. Pawlak, A.; Mucha, M. Thermochim Acta 2003, 396, 153.
25. Lee, D. K.; Kang, Y. S.; Lee, C. S.; Stroeve, P. J Phys Chem B 2002, 106, 7267.
26. Lee, J.; Isobe, T.; Senna, M. J Colloid Interface Sci 1996, 177, 490.
27. Saravanan P.; Alam, S.; Mathur, G. N. J Mater Sci Lett 2003, 22, 1283.